

## A new bend-magnet beamline for scanning transmission X-ray microscopy at the Advanced Light Source

Tony Warwick,<sup>a\*</sup> Harald Ade,<sup>b</sup> David Kilcoyne,<sup>b</sup> Michael Kritscher,<sup>a</sup> Tolek Tyliczszak,<sup>c</sup> Sirine Fakra,<sup>a</sup> Adam Hitchcock,<sup>c</sup> Peter Hitchcock<sup>c</sup> and Howard Padmore<sup>a</sup>

<sup>a</sup>Lawrence Berkeley National Laboratory, Berkeley, CA 94720, USA, <sup>b</sup>Department of Physics, North Carolina State University, Raleigh, NC 27695, USA, and <sup>c</sup>Brockhouse Institute for Materials Research, McMaster University, Hamilton, ON L8S 4M1, Canada. E-mail: warwick@lbl.gov

The high brightness of the bend magnets at the Advanced Light Source has been exploited to illuminate a scanning transmission X-ray microscope (STXM). This is the first diffraction-limited scanning X-ray microscope to operate with a useful count rate on a synchrotron bend-magnet source. A simple dedicated beamline has been built covering the range of photon energy from 250 eV to 600 eV. The beamline is always available and needs little adjustment. Use of this facility is much easier than that of installations that share undulator beams. This facility provides radiation for C 1s, N 1s and O 1s near-edge X-ray absorption spectromicroscopy with STXM count rates in excess of 1 MHz and with spectral resolution typically 1:2000, limited to about 1:5000.

**Keywords:** bend magnets; diffraction limit; zone plates; scanning microscopy; NEXAFS.

### 1. Introduction

A collaboration of scientists from North Carolina State University, Advanced Light Source, McMaster University, Dow Chemical Company and other institutions have built a dedicated scanning transmission X-ray microscope (STXM) for the study of the chemistry of heterogeneous polymeric materials by spatially resolved near-edge X-ray absorption spectroscopy (NEXAFS). This new scanning zone-plate microscope has been installed and is illuminated by means of a new bend-magnet beamline. In previous implementations of STXM (Kirz *et al.*, 1992; McNulty *et al.*, 1998; Kaulich *et al.*, 1999; Warwick, Ade *et al.*, 1998) the source has been an undulator. Earlier attempts to perform STXM on a bend magnet (Kirz & Rarback, 1985; Irtel von Brenndorff *et al.*, 1996) were of limited success because of the low count rate. In order to provide dedicated full-time operation for this polymer chemistry facility we have developed a bend-magnet beamline at the Advanced Light Source which is optimized for STXM. The required illumination intensity and spectral resolution have been achieved and the performance for STXM has been shown to be competitive with the existing undulator lines. This paper describes the design and performance of the bend-magnet beamline; a companion paper (Kilcoyne *et al.*, 2002) will describe the microscope.

### 2. Optical and mechanical design

The STXM zone-plate lens accepts only the coherent fraction of the illuminating beam when focusing at its diffraction limit. This coherent photon flux is inside a volume in transverse phase space of the order  $\lambda^2$ , incident on the lens and travelling close to the optical axis. Photons outside the phase-space acceptance are lost on slits and by overfilling the lens. This leads to a beamline design that is almost paraxial, with small optics and deep foci. The principles of the optical design have been described in an earlier publication (Warwick, Padmore & Ade, 1998).

A spherical-grating monochromator is adopted (Kirz *et al.*, 1992; McNulty *et al.*, 1998), dispersing in the horizontal plane and with geometry chosen for low dispersion. Operation is required from 250 eV (just below the C 1s NEXAFS range) to 600 eV (just above the O 1s NEXAFS range). C, N and O are the most important species in polymer chemistry. Fig. 1 shows the layout.

The horizontal dispersion plane leads to an overfilled entrance slit, because the horizontal illumination phase-space exceeds the diffraction limit by a large factor. The entrance slit can be opened to collect more light at the expense of spectral resolution. The low-dispersion design ensures that the grating defocus at the fixed exit slit is negligible over the operational range.

A toroidal mirror forms a horizontal image of the source at 0.9 magnification on the entrance slit. The entrance slit (at 300 eV) is typically 60  $\mu\text{m}$  wide in the horizontal direction, smaller than the image of the source. This slit width corresponds to a resolving power of about 2000. Higher resolution is available with smaller slits. The spherical grating forms a horizontal image of the entrance slit near the exit slit (which selects a specific value of photon energy). The exit slit is fixed in space. The grating rotation through the required energy range is only  $1.5^\circ$  (about a vertical axis). The grating focus coincides with the longitudinal position of the exit slit at two special values of the grating angle. Otherwise the grating is out of focus, but this does not appreciably affect the spectral resolution. Fig. 2 shows the computed flux into the acceptance of the zone-plate lens and the small reduction of the resolving power due to defocus. The grating horizontal magnification depends on the grating angle, ranging from 1.0 to 1.2.

In the vertical direction the toroidal mirror makes an image of the source at the exit slit. The exit slit (at 300 eV) is typically a square aperture,  $20 \times 20 \mu\text{m}$ , and acts as a source to be demagnified by the zone-plate lens. This aperture size diffracts to illuminate the lens with the full Airy disk or, in the language of Winn (Winn *et al.*, 2000), to an illumination parameter  $p = 1.0$ . Contrast for the highest spatial frequencies in an object improves markedly for  $p = 0.5$ , about half the aperture dimensions, with a corresponding reduction in flux.

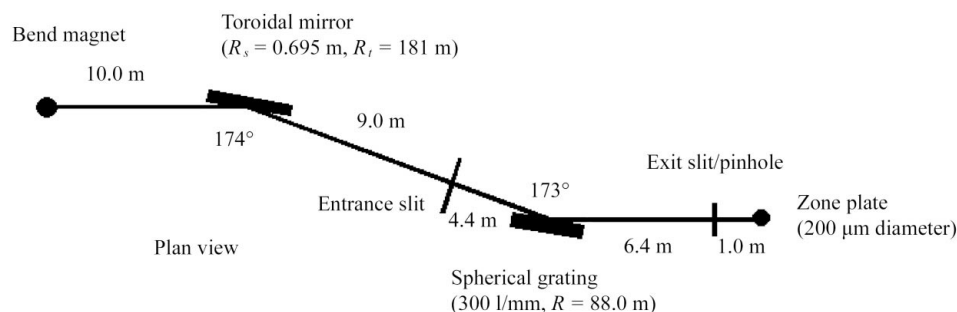


**Figure 1**  
Beamline layout (plan view).

Design parameters of the ALS handbook (PUB-643, revision 2, Lawrence Berkeley National Laboratory, USA) give a source size in the central bend magnet:

$$\sigma_x = 115 \mu\text{m} \text{ (0.1\% energy spread);}$$

$$\sigma_y = 9 \mu\text{m} \text{ (1\% emittance coupling).}$$

The bend-magnet source emits X-rays that, in the range 250 eV to 600 eV, are within vertical angles of about  $\pm 500 \mu\text{rad}$ . In the horizontal direction, of course, there is a uniform angular distribution through the deflection range of the bend magnet.

In the vertical direction the illumination from this source (at 300 eV) overfills the coherent phase space several times. The beam-line was designed to preserve the source vertical brightness so that this overfilling would occur on the exit slit and on the lens, easing the stringent alignment requirements. In practice the electron beam emittance and the emittance coupling of the ALS are smaller than the design value. As a result, the bend-magnet source is close to diffraction-limited in the vertical direction. However, the sagittal slope errors of the toroidal mirror are too large to preserve this higher brightness.

A specific beamline design goal was to independently trade off spatial resolution and spectral resolution for increased flux. This has been achieved in the following way.

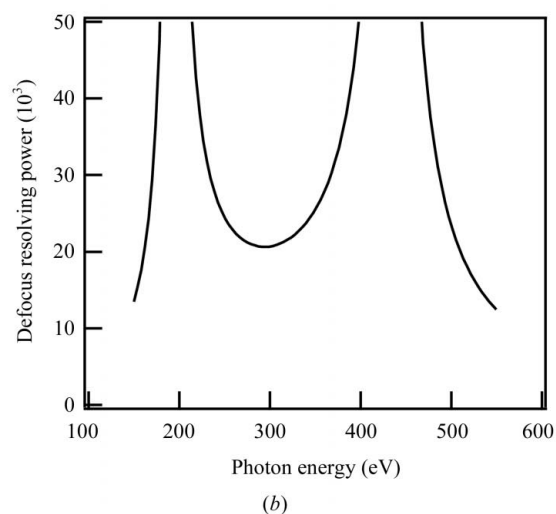
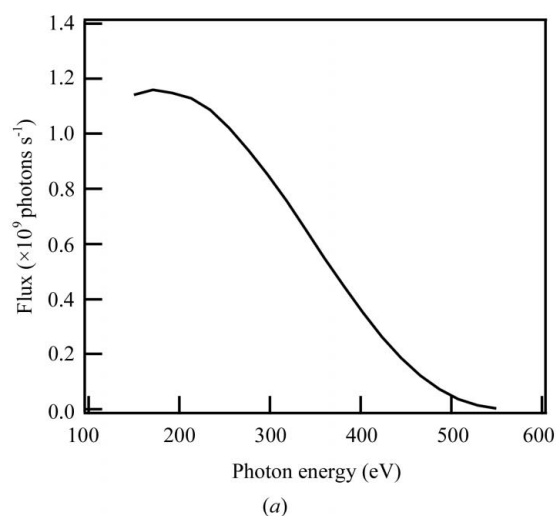


**Figure 2**

Computational results showing (a) flux transmitted into diffraction-limited phase space after the exit slit aperture, and (b) resolving-power contribution due to grating defocus.

In the horizontal direction the toroid accepts 1 mrad and the illumination overfills the coherent phase space by a factor of 65 (at 300 eV). The monochromator disperses in the horizontal plane so that some of the horizontal phase-space selection can be made at the entrance slit. This scheme allows the transmitted coherent flux to be increased by opening up the entrance slit and diffracting other wavelengths (from slightly off the axis) into the phase-space acceptance of the microscope. Thus the flux can be increased at the expense of spectral resolution without changing the imaging properties of the microscope.

The zone-plate lens in the microscope is positioned downstream of the exit slit. For diffraction-limited imaging the chosen demagnification requires the exit slit aperture to be about three times smaller than the vertical and horizontal aperture illumination. This is true for a spectral bandwidth of 1:2000. The flux loss at this undersized overfilled exit slit is recovered because the lens has been moved closer to demagnify less and therefore collects a larger solid angle, so there is no penalty. However, the microscope can now accept almost an order of magnitude more photons when the exit slit is opened by a factor of three in both directions. Thus the flux can be increased at the expense of spatial resolution without changing the spectral resolution.

The monochromator mechanism is extremely simple, with one grating held in a 15 cm vacuum cube, rotating about flexural pivots outside the vacuum. There is a motorized sine-bar 0.5 m long with a linear encoder at the end with 0.1  $\mu\text{m}$  resolution.

Steering over a small angular range is provided by means of two piezo actuators on the toroidal mirror. This is crucial. A slow servo loop is required to maintain beamline throughput by locking the mirror steering onto the entrance slit (horizontal) and the exit slit (vertical).

The sagittal slope errors of the polished toroid turned out to be 12  $\mu\text{rad}$  r.m.s. and are not negligible. They degrade the vertical brightness by a factor of about three, blurring the image on the exit slit in the vertical direction and reducing the transmitted coherent flux, but easing the alignment requirements.

The spherical glass diffraction grating has a laminar profile, with 300 lines  $\text{mm}^{-1}$ , a groove width of 1.8  $\mu\text{m}$  and a groove depth 19 nm. The measured diffraction efficiency of this grating in first order has a maximum at 300 eV with a value of 28%, in very close agreement with the design computations.

### 3. Performance

Fig. 3 shows the measured flux through a small silicon nitride window into a phase space acceptance similar to that of the zone-plate microscope. These measurements were made with a silicon detector, corrected for the energy-dependent quantum efficiency (3.6 eV per ion/hole pair). Except for the effects of the silicon nitride window, the measurements can be compared directly with the computed flux shown in Fig. 2. The corresponding spectral resolution is about 1:2000 across the complete range of photon energy. The measured flux is reduced by about a factor of four below the computed values by the vacuum window absorption and the effect of the sagittal slope errors of the toroid. After further reductions due to zone-plate window absorption, zone-plate diffraction efficiency and photon-counting detector efficiency, the microscope count rates are of the order of 1 MHz under diffraction-limited conditions.

These flux measurements also illustrate the success we have had keeping the beamline clean during assembly. Since most of the work will be at the carbon *K*-edge we attached great importance to this. There are 'Viton'-sealed gate valves in the line, but no other

hydrocarbons. All components are carefully degreased, electro-polished if possible, and the components of the two optical assemblies are vacuum-baked at 593 K before assembly. Optics arrive clean from the vendors; they are merely rinsed with solvent. Absorption by the carbon layer on the two optical surfaces reduces the flux by about 15% at 300 eV. We have found that beamlines which start as clean as this can stay clean for years.

There is presently a significant amount (perhaps 20%) of light at twice the selected energy, diffracted from the grating in second order. This higher-energy component shows up (at 530 eV) as an O<sub>2</sub> absorption dip at the 265 eV setting of the monochromator. Note that the silicon detector emphasizes this component by a factor of two because these photons have twice the energy. This second-order light can be removed by an N<sub>2</sub> gas filter which has not yet been installed. The windowless differentially pumped filter has four small apertures through which the useful beam must be threaded without loss. Third-order light above 800 eV is suppressed by the nickel optical coatings on both optical surfaces. The oxygen absorption in the beamline is from oxidation of the nickel.

Fig. 4 shows the illumination profile at the approximate location of the zone plate. Both the horizontal and vertical sizes are less than expected by about 25%. This may be due to an inaccurate deflection angle off the toroidal mirror. However, the zone plate is filled with light and there is no penalty.

Fig. 5 shows gas-phase absorption spectra made as resolution tests with narrow slits. These spectra are from CO (C 1s), N<sub>2</sub> (N 1s) and O<sub>2</sub> (O 1s). The key to achieving high resolution was to adjust the included angle at the grating by moving the exit slit sideways by several centimeters, to the point where the defocus effects are minimized. 10 cm of CO at 20 mtorr was measured at 287 eV and the spectra fitted with a Gaussian width of 57 meV and a Lorentzian width of 95 meV. 10 cm of air at 50 mtorr was measured at 401 eV and the spectra fitted with a Gaussian width of 75 meV and a Lorentzian width of 110 meV. The maximum resolving power of the beamline is higher than 5000. Note that typical operation is at a resolving power of  $R = 2000$  with count rates of the order of 1 MHz, corresponding to Fig. 3 as described above. For operation at  $R = 5000$  the entrance and

exit slit-widths are reduced in the dispersive direction and the count rate is reduced by a factor of about 6.25 to values of the order of 160 kHz.

#### 4. Spatial resolution

The development of a new scanning microscope for X-ray imaging and NEXAFS spectromicroscopy is nearing completion at this beamline. Fig. 6 shows a test pattern image close to the zone-plate diffraction limit with a count rate of about 1 MHz. This is a pattern of transparent lines drawn in an opaque gold coating deposited on a silicon nitride window. The line-to-space ratio is 1:1 and the transparent lines are 40 nm apart. An interferometer servo loop is active, locking the position of the stage, during scanning, to give the correct momentary relationship between the transverse position of the sample and the zone-plate lens. This scheme is effective against thermal drifts, low-frequency vibrations and dynamic image distortion. The zone plate used for this image had an outermost zone width of 40 nm. Detailed analysis of these and similar images or other test patterns indicate that the spatial resolution is close to the theoretical diffraction-limited resolution of the zone plate. We hope to obtain better spatial resolution in the future with better zone plates. More analysis of the microscope performance will be given in a separate paper (Kilcoyne *et al.*, 2002).

#### 5. Conclusions

This project has provided a dedicated spectromicroscopy capability with reliable and reproducible illumination. The illumination flux and the spectral resolution are perfectly adequate for all scanning transmission X-ray microscopy measurements. The success of this project represents a new approach at the ALS in which high-brightness experiments are installed on simple dedicated bend-magnet lines. Enormous gains in productivity are expected from experimental facilities illuminated in this way, with experimenters free of the need to operate a complicated beamline and free of the constraints of shared use, which would involve retuning the beamline.

Thanks to E. Gullikson for assistance with diffraction-grating efficiency measurements and to S. Irick for optic metrology. Thanks

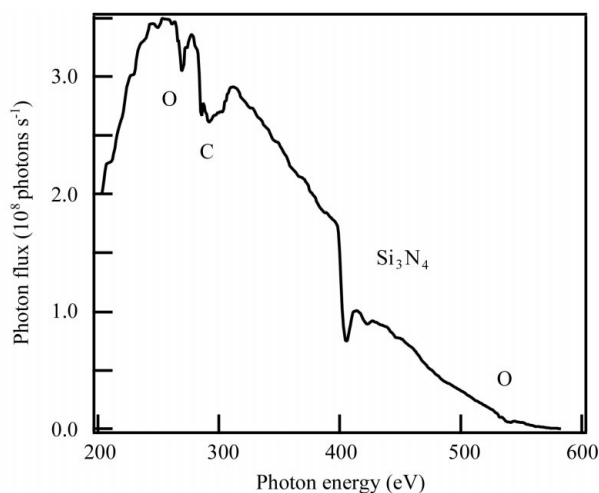


**Figure 3**  
Measured flux transmitted into the diffraction-limited phase space through a 100 nm-thick Si<sub>3</sub>N<sub>4</sub> window after the exit slit aperture. The flux is measured with entrance and exit slits changing as  $1/E$  ( $60 \times 20 \times 20 \mu\text{m}$  at 300 eV). This keeps the spectral resolution approximately constant at about  $R = 2000$  and keeps the exit slit aperture size matched to the diffraction limit of the fixed zone-plate lens.

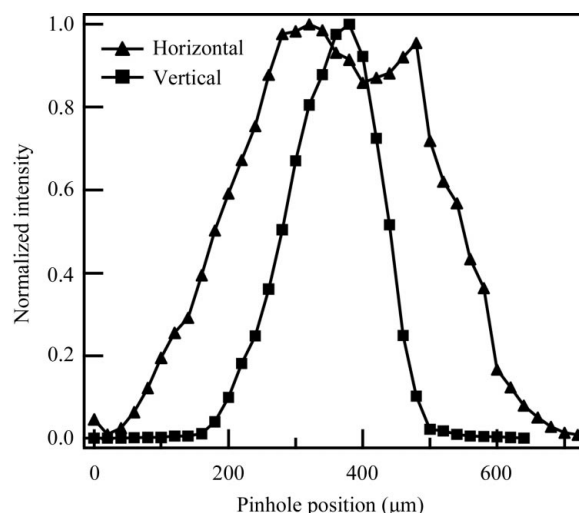


**Figure 4**  
Horizontal and vertical beam size near the zone-plate position (60 cm downstream from the exit slits) measured with a  $50 \mu\text{m}$  pinhole at 395 eV.

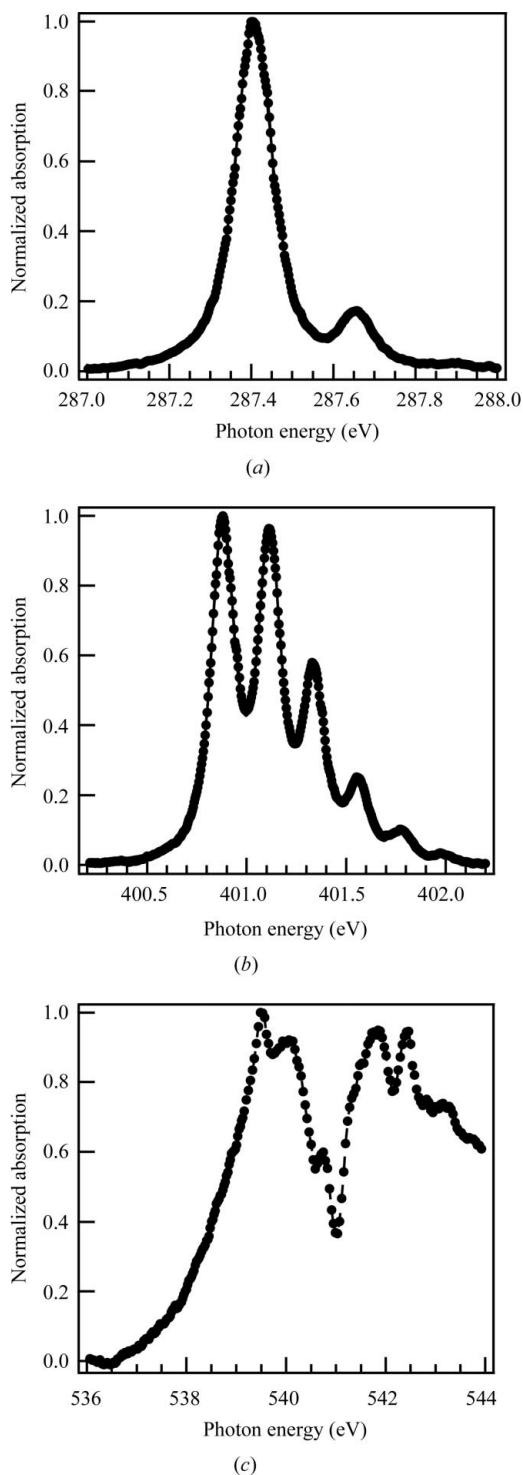


**Figure 5**  
 Gas-phase absorption measurements as tests of spectral resolution. (a) Vibrationally resolved  $C\ 1s \rightarrow \pi^*$  transition in CO. (b) Vibrationally resolved  $N\ 1s \rightarrow \pi^*$  transition in  $N_2$ . (c) Rydberg fine structure in  $O_2$ .

to Frank Zucca, John Pepper and the other members of the ALS vacuum group. This work was supported by the Director, Office of

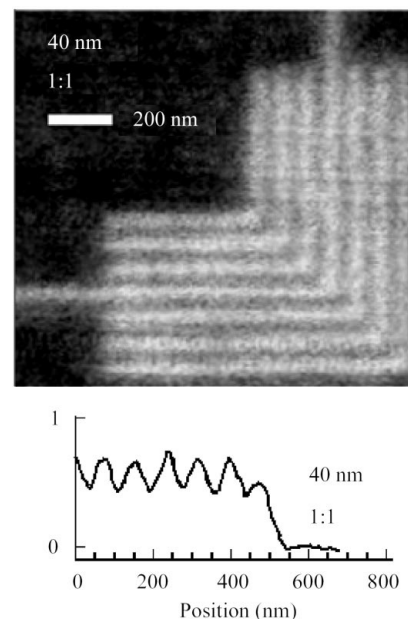


**Figure 6**  
 X-ray image of a test pattern with 40 nm lines, spaced 40 nm apart. An average of the line profiles across the lines is shown on a normalized intensity scale. The zone plate and test pattern have been prepared by Erik Anderson, Bruce Harteneck *et al.* (CXRO, LBNL).

Energy Research, Office of Basic Energy Sciences, and Materials Sciences Division of the US Department of Energy, under Contract No. DE-AC03-76SF00098 and DE-FG02-98ER45737. The work of AH is supported by NSERC and the Canada Research Chair program.

## References

- Irtel von Brenndorff, A., Niemann, B., Rudolph, D. & Schmahl, G. (1996). *J. Synchrotron Rad.* **3**, 197–198.
- Kaulich, B., Oestreich, S., Salome, M., Barrett, R., Susini, J., Wilhein, T., Di Fabrizio, E., Gentili, M. & Charalambous, P. (1999). *Appl. Phys. Lett.* **75**, 4061–4063.
- Kilcoyne, A. L. D., Tyliszczak, T., Steele, W. F., Hitchcock, P., Fakra, S., Frank, K., Rightor, E., Mitchell, G., Anderson, E., Harteneck, B., Hitchcock, A., Yang, L., Warwick, T. & Ade, H. (2002). In preparation.
- Kirz, J., Ade, H., Jacobsen, C., Ko, C.-H., Lindaas, S., McNulty, I., Sayre, D., Williams, S., Zhang, X. & Howells, M. (1992). *Rev. Sci. Instrum.* **63**, 557–563.
- Kirz, J. & Rarback, H. (1985). *Rev. Sci. Instrum.* **56**, 1–4.
- McNulty, I., Frigo, S. P., Retsch, C. C., Wang, Y., Feng, Y. P., Qian, Y., Trakhtenberg, E., Tieman, B., Cha, B. C., Goetze, K., Mooney, T. & Haddad, W. S. (1998). *Proc. SPIE*, **3449**, 67–74.
- Warwick, T., Ade, H., Cerasari, S., Denlinger, J., Franck, K., Garcia, A., Hayakawa, S., Hitchcock, A. P., Kikuma, J., Klinger, S., Kortright, J., Meigs, G., Morisson, G., Moronne, M., Myneni, S., Rightor, E., Rotenberg, E., Seal, S., Shin, H.-J., Steele, W. F., Tyliszczak, T. & Tonner, B. P. (1998). *Rev. Sci. Instrum.* **69**, 2964–2973.
- Warwick, T., Padmore, H. A. & Ade, H. (1998). *Proc. SPIE*, **3449** 12–18.
- Winn, B., Ade, H., Buckley, C., Feser, M., Howells, M., Hulbert, S., Jacobsen, C., Kaznacheyev, K., Kirz, J., Osanna, A., Maser, J., McNulty, I., Miao, J., Overluisen, T., Spector, S., Sullivan, B., Wang, Yu., Wirick, S. & Zhang, H. (2000). *J. Synchrotron Rad.* **7**, 395–404.